Available online at www.sciencedirect.com
SCIENCE DIRECT®
Earth and Planetary Science Letters 243 (2006) 128–140
EPSL
www.elsevier.com/locate/epsl

Enclaves provide new insights on the dynamics of magma mingling: A case study from Salina Island (Southern Tyrrhenian Sea, Italy)

Guido Ventura [a,*], Piero Del Gaudio [a], Gianluca Iezzi [b]

[a] *Istituto Nazionale di Geofisica e Vulcanologia, Roma, Italy*
[b] *Dipartimento Scienze della Terra, Universitá di Chieti, Chieti, Italy*

Received 25 October 2005; received in revised form 19 December 2005; accepted 4 January 2006
Available online 7 February 2006
Editor: S. King

Abstract

Three lava flows (hereafter, flows A, B, and C) from Salina Island (Italy) consist of basaltic andesitic enclaves dispersed in a dacitic matrix. Enclaves represent 8–12 vol.% of the erupted magma. The number of enclaves and the surface covered by the enclaves at each outcrop do not vary significantly with the distance from the vent in the flows A and B. These feature reflect the dynamics of magma mingling within the reservoir and not the kinematics of the lava flow. In the flow C, these parameters vary irregularly. The statistical entropy $S(t)$ of the enclaves, which is a measure of their spatial distribution (dispersion), is estimated in outcrops located at different distance from the vent. The Kolmogorov–Sinai entropy rate k, which describes the variations of $S(t)$ with time, is also determined. In the lava flow A, $S(t)$ increases linearly with time t for $0<t<0.4$; k is 0.04. For $t>0.5$, $S(t)$ attains its maximum value and maintains constant with increasing t. In the lava flow B, $S(t)$ linearly increases with t, and k is 0.01. In the lava flow C, there is not correlation between $S(t)$ and t. The comparison between the results from the analysis of the Porri enclaves and those from numerical experiments on the variation of $S(t)$ in chaotic advective mixing systems and from previous experimental models on magma mixing, allow us to draw some conclusions on dynamics of the basaltic andesite–dacite mingling in the magma chamber. Fully chaotic magma mingling systems show three evolution stages. An initial stage, which is unknown because of the disruption of the initial configuration of the interacting magmas, a second stage characterized by a linear increase of the statistical entropy with time, and a third stage, in which the uniformity of the system is reached, and the entropy does not vary with increasing time. A system in which the uniformity is never attained, is characterized by irregular variations of $S(t)$ with time. In the flows A and B, the relations between $S(t)$ and t are consistent with those of a fully chaotic dynamics possibly associated to convection. The basaltic andesite was uniformly distributed in the dacitic host due to the occurrence of convective movements driven by the injection of the basaltic andesite within the dacitic chamber. The mingling system recorded by the lava flow A evolved with a higher rate with respect to that of the flow B. This suggests that chaotic advection (stirring and folding) is more efficient in the magmatic system A than in B. On the contrary, the mingling system C is characterized by a non-uniform distribution of the basaltic andesite within dacite. This reflects the occurrence of a dynamics in which stirring and folding processes do not operate efficiently and are unable to uniformly distribute the dispersed phase within the continuous one. The decrease of k from A to B, and the lack of a measurable k in C, along with the observation that A and B were emitted before C, indicate that the efficiency of advective movements within the Porri magma chamber declined with decreasing time. Mingled magmas characterized by a homogeneous spatial distribution of enclaves or an initially inhomogeneous distribution evolving towards a homogeneous one are indicative of efficient advection processes that may

* Corresponding author. Istituto Nazionale di Geofisica e Vulcanologia, Department of Seismology and Tectonophysics, Via di Vigna Murata 605-00143 Roma, Italy. Tel.: +39 06 51860221; fax: +39 06 51860565.
E-mail address: ventura@ingv.it (G. Ventura).

doi:10.1016/j.epsl.2006.01.004

favor magma mixing. Mingled magmas characterized by an inhomogeneous distribution of enclaves suggest low dynamical interaction between the two end-members. Magma mixing is not allowed.

Keywords: volcanology; petrology; magma mingling; enclaves; lava flows; entropy

1. Introduction

Enclaves have been recognized in plutonic and volcanic rocks, and their occurrence indicates the physical interaction (mingling) between magmas of different composition [1–4]. Geochemical and structural studies on enclaves are abundant [4–8] and references therein], and allow us to reconstruct the processes responsible for the mingling of magmas, which include: injection of mafic magma into a silicic one, disruption of the stratification of a magma chamber during eruption, vesiculation of a mafic magma within a densely stratified reservoir, floating of a layer of mafic magma into a more evolved magma due to vesiculation, or to coupled vesiculation and crystallization, and disruption of a solid layer of mafic magma.

According to results from fluid-dynamical experiments on immiscible liquids [9,10], recent studies suggest that chaotic advection, i.e., efficient stirring/stretching and folding, plays an important role in the dynamics of magma mingling [11–13]. The main evidence of chaotic advection is the coexistence, within the same magmatic body and at different length scales (10^{-4}–1 m), of enclaves characterized by a fractal structure and by morphological features similar to those recognized in chaotic systems, i.e., vortexes, folds and stirring structures. However, natural dynamical systems are not necessarily chaotic. Also, they may be characterized by different degrees of chaos [14,15]. In statistical mechanics, the degree of chaos of a dynamical system can be estimated analyzing the time evolution of two key-parameters [16–22]: the statistical entropy S, which is a measure of the spatial distribution (dispersion) of a system, and the Kolmogorov–Sinai entropy rate k, which describes the dynamic instability of trajectories in the phase space.

In this study, we analyze the spatial distribution of the enclaves hosted in three lava flows from the Porri volcano (Salina Island, Southern Tyrrhenian Sea, Italy). We determine the statistical entropy of the enclaves within these lavas at different distances from the vent, and calculate k. The collected data are discussed in light of results from numerical experiments and allow us to (a) provide a description of the time and spatial evolution of enclaves within their host, (b) have a relative estimate of the degree of chaos of the magma mingling system, and (c) discriminate between different chaotic dynamics within the magma chamber.

The paper is organized as follows. In a first section we describe the geological and geometrical features of the selected lava flows and enclaves. In the second section we present the theory on the evolution of S and k in chaotic mixing systems using numerical experiments. In the third section, we illustrate the analytical method used to determine S and k in the Porri lavas using enclaves. In the last two section, we present and discuss the results, and summarize the most relevant conclusions.

2. Geological setting and general features of the selected lava flows with enclaves

Salina Island (Southern Tyrrhenian Sea, Italy) consists entirely of volcanic rocks related to the activity of five main volcanoes emplaced between 430 and 13 ka (Fig. 1a [23–25]). Porri volcano (865 m a.s.l.) is located in the western part of Salina, and consists of 83 to 43 ka old lava flows and scoria fall deposits [25]. The composition of the Porri products ranges from basaltic andesites to dacites [24].

Most of the Porri lavas are texturally heterogeneous. They are characterized by the occurrence of dark enclaves hosted in a lighter matrix (Fig. 1b). Here, we select three of these lava flows, which outcrop in the southern sector of the Porri volcano (lava flows A, B and C in Fig. 1a). These lavas were emitted from the Porri crater during the last phase of activity of the volcano, which date back to about 43 ka. On the basis of the field relationships, the lava flows A and B were emitted before the flow C. Geochronological data on the selected lavas flows are unavailable and the time interval between the three effusive episodes cannot be estimated. The structural and geochemical features of the Porri lavas, as well the physical properties of the two interacting magmas, were extensively described in previous studies [26–29] and only the main features are reported here.

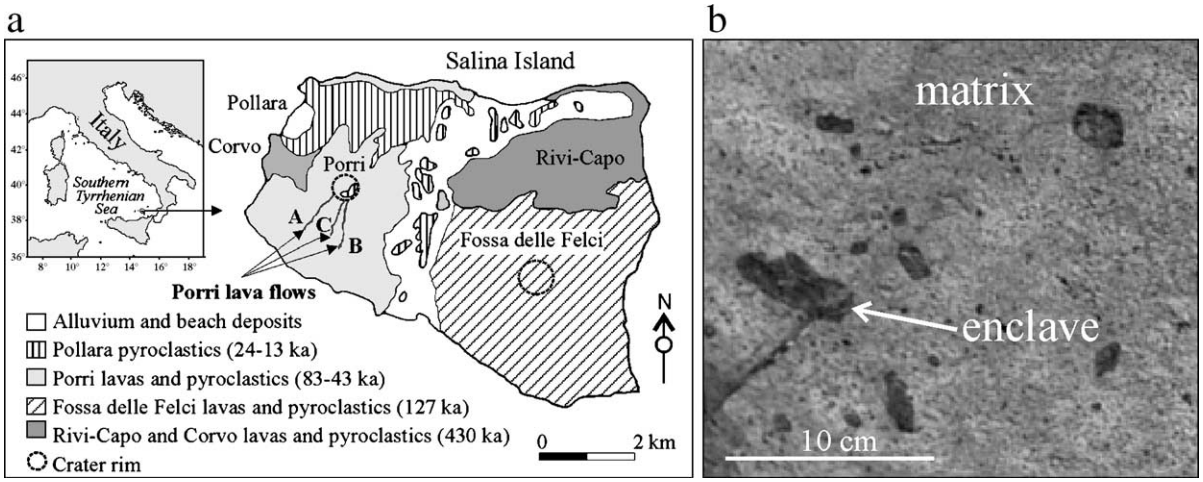

Fig. 1. (a) Geological sketch map of Salina Island (simplified from Barca and Ventura [24]) with location of the lava flows A, B and C. (b) Field relationships between the basaltic andesitic enclaves and the dacitic matrix in the lava flow C.

Similar morphological, structural and geochemical features characterize the lava flows A, B, and C. These lavas lie on a 6° to 14° dipping substratum constituted by older flows. Lava flows A and B have an exposed length of about 1 km, whereas the lava flow C has a length of about 800 m (Fig. 1a). The width of the flows ranges between 5 and 21 m and the thickness is between 2.5 and 4 m. In sections containing the flow direction and orthogonal to the surface on which the flow moved, the lavas consists of three main portions. The basal and upper portions are 0.5 to 1 m thick, and are made up of scoriaceous breccias (a′a-type lava). The middle portion is massive and texturally heterogeneous. Dark enclaves (Fig. 1b) are hosted in a crystal-rich matrix pink in colour. The enclaves of the lava flows A, B and C are characterized by circular to ellipsoidal shapes. On the outcrop, the size of the enclaves ranges from few mm^2 to 35–40 cm^2. The enclaves are vesicle-free, whereas the vesicle content of the matrix is between 0 and 5 vol. %. The enclaves represent 8–12% of the exposed surface, and have a crystal content ranging from 15 to 20 vol.% (cpx, opx, plg, ox and ol). The glass has a basaltic andesitic composition (SiO_2=53–55.5 wt.%; K_2O=1.20–1.54 wt.%; [26,30]). The matrix in which the enclaves are hosted has 45–51 vol.% of crystals (cpx, opx, plg, ox and amph) and a high-potassium dacitic glass composition (SiO_2=61.25–64.11 wt.%; K_2O=2.32–2.61 wt.%; [26,30]).

According to Colleta, De Rosa et al., and Ventura [26–30], the enclaves of the Porri lavas reflect the arrival of a basaltic andesite in a shallower reservoir where a resident, crystallizing high-potassium dacitic magma is stored. Following Zanon [31], the shallower storage zone is located between 1.3 and 2.8 km, while the deeper magma comes from a depth larger than 12 km. The lack of mixing (hybridization) processes between the basaltic andesite and the high-potassium dacite is due to the different rheological properties of the two magmas (Table 1) [29,30]: the ratio between the viscosity of the basaltic andesite and that of dacite is $\sim 10^{-2}$, and the ratio between the yield strengths is ~0.38 [29].

As already recognized in other lavas from the Porri and other volcanoes [29,32], the smaller enclaves of the lava flows A, B and C are less deformed of the larger ones. According to Williams and Tobish [33], the deformation of a drop is proportional to the Capillary number, which is the ratio between the viscous stress

Table 1
Viscosity, yield strength, density, water content and temperature of basaltic andesite (enclaves, dispersed phase) and dacite (continuous phase)

Magma	Viscosity (Pa s)	Yield strength (Pa)	H_20 (wt.%)	Density (kg/m^3)	Temperature (°C)
Dacite	1.35 10^6	85	2.0	2570	950
Basaltic andesite	1.20 10^4 (5.3 10^3)	33	0.5	3200 (2900)	950 (1050)

Values in parentheses refer to 1050 °C. Data from Colleta, De Rosa et al., Ventura et al., and Ventura [26–30].

and the interfacial tension. This number is, in turn, proportional to drop size. As a result, smaller drops deform less than the larger ones. Also, freezing processes may affect the enclaves, and the smaller enclaves form a chilled margin earlier than the larger ones [32]. We cannot establish which of these two processes prevails within the selected Porri lava flows A, B, and C. However, as suggested by Ventura [29], and independently from the drop size and presence or not of chilled margins, the trajectories of the basaltic enclaves in the dacitic magma are imposed by the kinematics of the host. On the basis of these observations, and taking into account that the enclaves represent a low fraction (0.08–0.12) of the lavas, the enclaves are passive markers whose spatial distribution in controlled by the flowing matrix.

3. Statistical entropy and entropy rate in chaotic advection

A convenient numerical description of a conservative (constant volume), advective mixing system is the 'standard map', also known as Taylor–Greene–Chirikov map [22]. The map is defined by the following iterative rule:

$$x_{n+1} = x_n + y_{n+1} \quad [\text{mode I}] \tag{1a}$$
$$y_{n+1} = y_n + a/2\pi\sin(2\pi x_n) \quad [\text{mode I}] \tag{1b}$$

where a is a control parameter. x_n, y_n and x_{n+1}, y_{n+1} are the coordinates of a particle at the dimensionless time $t=n$ and $t=n+1$, respectively. Eqs. (1a,b) forms a two-dimensional system where the [mod 1] statement means that the domain of the system is periodic between zero and one ($0<(x,y)<1$). In the map, the amount of chaotic advection increases with a [17–19]. In particular, increasing a values correspond to increasing the efficiency of stretching and folding processes. As pointed out by Perugini et al. [12], the flow scheme of Eqs. (1a,b) is useful for simulating advection during fluid mixing and, in particular, during mixing of magmas because a variety of flow behaviors in pipe-flows, shear flows, convective flows, can be obtained by varying parameter a.

As an example, consider a unit square whose space is occupied by an initial, very localized, distribution of 5000 particles (Fig. 2, top), and analyze the time evolution of these particles in the phase space by setting $a=1$, $a=5$, and $a=10$ in Eqs. (1a,b). According to the Liouville's theorem [22], the number of particles in the phase space is constant with time.

Results of the numerical experiments are reported in Fig. 2. For $a=1$ (Fig. 2a), the distribution weakly stretches and folds. The distribution is strongly anisotropic and the particles never homogeneously occupy the available phase space. For $a=5$ (Fig. 2b), the amount of stretching and folding increases with respect to the configurations with $a=1$. As the time (iteration) increases, the points tend to occupy the available phase space, but zones characterized by higher concentrations may be easily recognized. For $a=10$ (Fig. 2c), the amount of stretching and folding is larger with respect to that observed in the maps with $a=1$ and $a=5$ at iterations 2 and 4. As the time increases, the distribution occupies the whole phase space.

The statistical entropy S of the distributions reported in Fig. 2 is calculated using the procedure adopted by Baranger et al. [19]. The phase space is divided into a grid $M=10\times10$ cells and the entropy $S(t)$ is determined by:

$$S(t) = -\sum_{i}^{M} p_i(t)\log p_i(t) \tag{2}$$

where $p_i(t)$ is the probability that the state of the system falls inside cell c_i of the phase space at time t. Note that $S(t)$ may be positive or negative. Fig. 3 shows the variation of the statistical entropy with time of the standard maps depicted in Fig. 2 and an additional map with $a=2$. For the maps with $a=5$ and $a=10$, there is a linear increase of the entropy from the initial stage up to iterations 4 and 3, respectively (dashed lines in Fig. 3). The slope of this linear portion of the curves is the Kolmogorov–Sinai entropy rate $k=\mathrm{d}S/\mathrm{d}t$, which is a measure of the mixing properties of chaotic systems, being proportional to the rate of the system to reach the homogeneity of the phase space [17]. At iterations larger than 7, the curve for $a=10$ reaches a constant, maximum value ($S(t)=20$), and the phase space is homogenously occupied. In this system, the chaotic advection plays an important role because, after few iterations, the spatial uniformity is achieved. It is worthy of note that the maximum value of the entropy of a chaotic dynamical system is a function of the number of points within the system and of the initial distribution. The curve with $a=5$ approaches asymptotically a constant value, which, however, is never attained. The phase space is near to be uniform, but the complete homogenization is not attained. For $a=2$, $S(t)$ increases non-linearly up to iteration 9, and irregularly vary between -1.39 and -2.46 (Fig. 3). The curve of variation of the entropy with time for $a=1$ (Fig. 3) shows irregular oscillations of $S(t)$ with

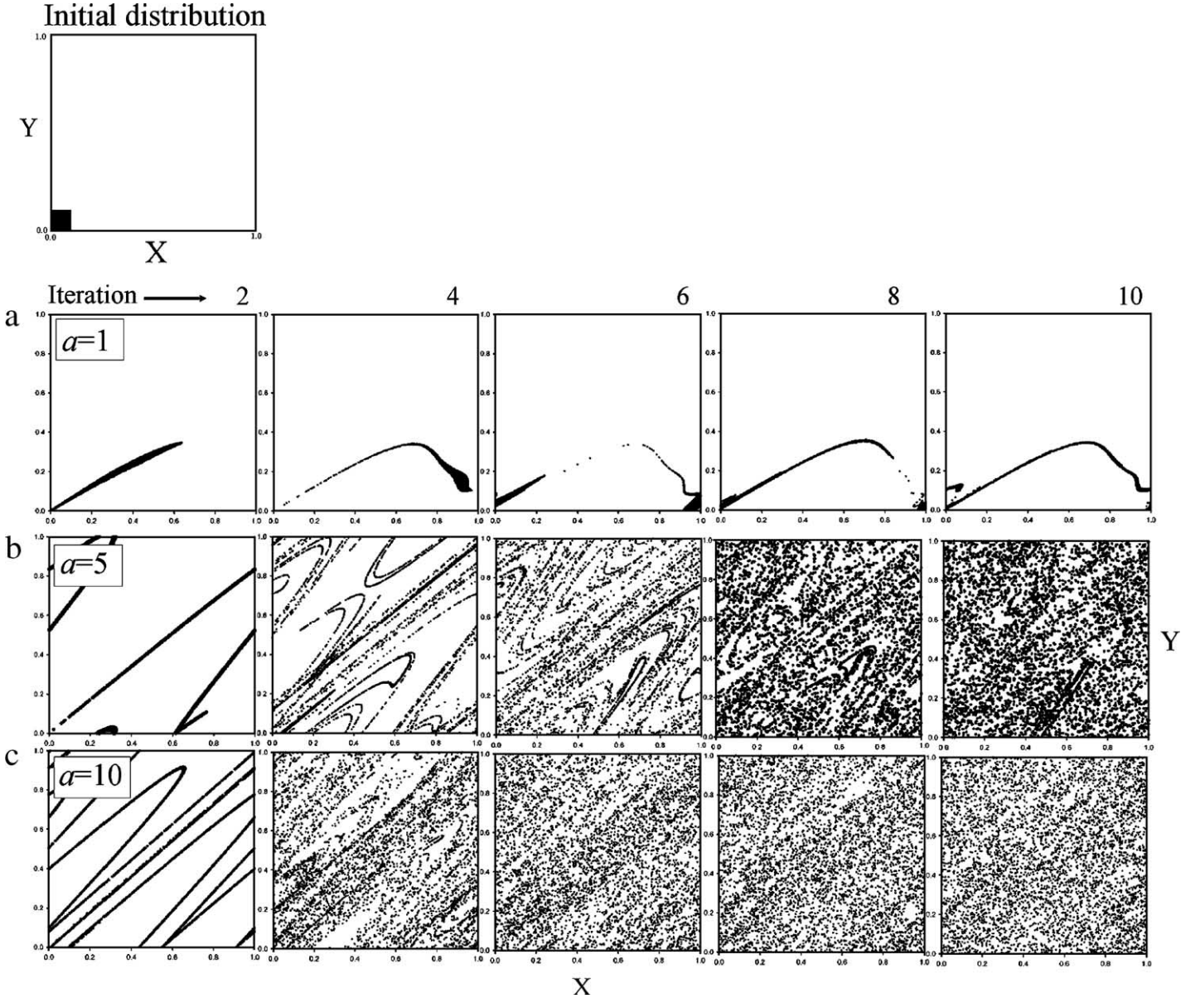

Fig. 2. Time evolution of an initial configuration of 5000 particles (top, left) using the 'standard map' (Eq. (1a,b)), with (a) $a=1$, (b) $a=5$, and (c) $a=10$.

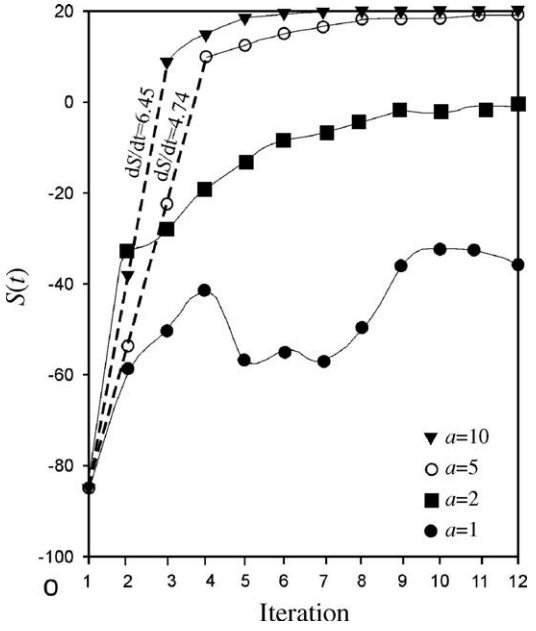

Fig. 3. Time evolution of $S(t)$ in the standard map with $a=1$, $a=2$, $a=5$, and $a=10$. Dashed line marks the linear portion of the curves. Continuous lines are spline interpolations.

time, and a positive (or negative) linear relation between $S(t)$ and t cannot be defined. An asymptotic trend is also lacking. These features indicate that, for $a=1$, the mixing system is far from the uniformity [21], and chaotic advection does not play an important role.

Results from Fig. 3 and theoretical studies [16–21] show that the time evolution of the statistical entropy in chaotic, conservative mixing systems follows three main stages: (1) in the first stage, at the beginning of the mixing process, $S(t)$ is dependent on the details of the dynamical system and of the initial distribution; (2) in the second stage, as the mixing process advances, $S(t)$ is a linear increasing function whose slope is k; (3); in the third stage, $S(t)$ tends asymptotically toward a constant value for which the distribution is uniform. This three-stage evolution characterizes a strong chaotic regime, where a significant portion of the available space or the whole space is characterized by a spatial uniformity. In a such system, stirring and folding processes operate efficiently and distribute homogenously the dispersed phase within the continuous one. In a regime where only a small portion of the available phase space is characterized by chaotic mixing, the statistical entropy varies irregularly with time. Stirring and folding processes do not operate efficiently and the dispersed phase remains concentrated in the some portions of the available space.

4. Analytical methods

The procedure adopted for the estimate of the statistical entropy and entropy rate using enclaves from the Porri lava flows A, B, and C, may be summarized in the following points.

1. We select outcrops of the lava flows at different distance from the vent. These outcrops are vertical sections that are orthogonal to the substratum on which the flow moved and contain the flow direction. Each outcrop measures at least 1×1 m. The number of outcrops satisfying these criteria is 23 for the lava flow A, 18 for the flow B, and 21 for C.
2. Where possible, we take photos of the outcrop using a digital camera (Fig. 4a), and correct distortion effects throughout orthorectification. Then, the enclaves with linear size >2 cm are selected and the x and y coordinate of each enclave is recorded within a 1×1 m reference square (Fig. 4b) using the Scion Image 4.02 software by Scion Corporation. Where not possible, the coordinates are taken directly in the field using the same reference square. Errors between the two procedures of acquisition are less than 2.5 and 3.2 cm for the x and y coordinate, respectively. A map of the x–y position of the enclaves within the reference square is then constructed (Fig. 4b), and the number of points (enclaves) within each square is measured. The surface covered by the enclaves has been also measured.
3. For the determination of $S(t)$, we divide each 1×1 m square in 20×20 cm cells (Fig. 4b), and count the number of points within each cell. Since the value of $S(t)$ (Eq. (2)) depends on the number of points, we normalize $p_i(t)$. The normalized probability $p_{ni}(t)$ within each cell is:

$$p_{ni}(t) = (n_c/n_{totc})/M \tag{3}$$

where n_c is the number of points within a cell, n_{totc} is the total number of points within the 1×1 m square, and $M=25$ is the number of cells within the square (see Fig. 5b).
4. For the determination of the entropy rate, which is the variation of $S(t)$ with t, we convert the distance of the outcrops from the vent in dimensionless time using velocity. To have a quantitative estimate of the flow velocity V of the three lavas, we use the Jeffrey's equation:

$$V = \rho g d^2 \sin\theta / 3\eta \tag{4}$$

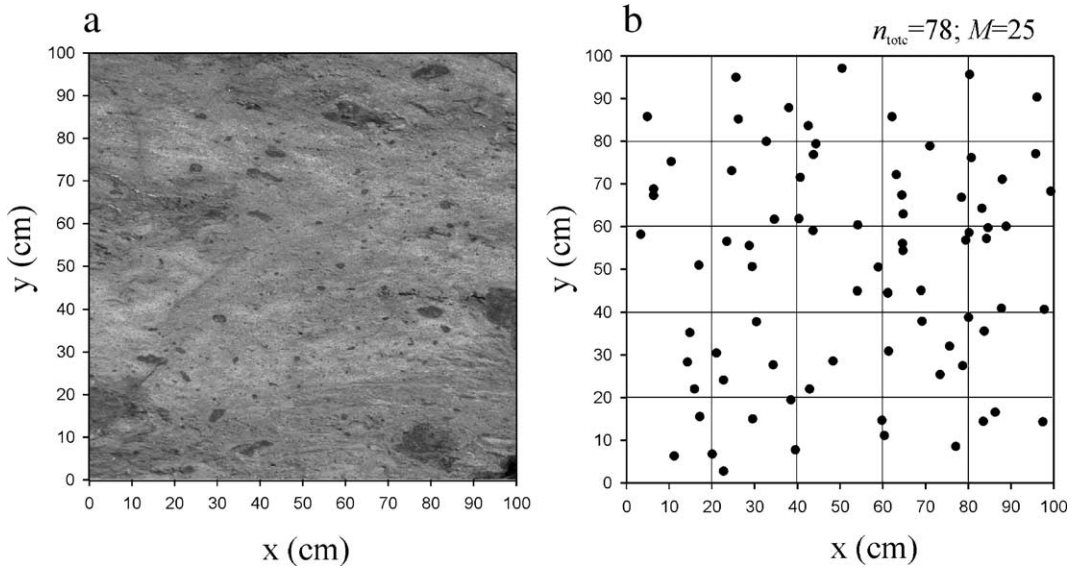

Fig. 4. Example of the procedure adopted to map the enclaves within a 1×1 m outcrop. (a) Digital photo of the outcrop (lava flow C, 450 m from the vent). (b) Gridding of the outcrop and x–y position of the enclaves with linear size ≥2 cm. n_{ctot} is the number of enclaves in the outcrop, and M is the number of cells in the grid.

where ρ is the density of the magma (crystals plus melt), g is the acceleration of gravity, d is the thickness of the lava flow, θ is the underlying slope, and η is the viscosity of the magma. We apply Eq. (4), which is valid only for Newtonian fluids and not for Bingham fluids, because: (a) some parameters required for Bingham fluids, e.g., the critical thickness before the flow will move, cannot be estimated for the Porri lavas, (b) the time of emplacement will be expressed as dimensionless time (see below). To determine V using Eq. (5), the viscosity and the density of the Porri lavas are determined using a subroutine of *Conflow* [34]. We select a dacitic composition, 50 vol.% of crystals, a temperature of 950 °C, and H_2O=2 wt.% [30]. The obtained viscosity is 1.35 10^6 Pa s, and the density is 2570 kg m^{-3}. Using d=3 m and θ=10°, V is ~25 m/h. Because of the near constant thickness of the three selected Porri lavas and lack of abrupt changes in the underlying slope, we assume that the velocity of the three flows was constant during the emplacement. The value of velocity determined using Eq. (5) suggests that the lavas A and B emplaced in about 40 h, whereas the flow C emplaced in about 32 h. The dimensionless time t_n is estimated as:

$$t_n = (l/V)/t_e \quad (5)$$

where l (m) is the distance from the lava flow front of each outcrop, V=25 m/h, and t_e=40 h. The calculated normalized entropy $S_n(t)$ of each map is then:

$$S_n(t) = -\sum_{i}^{25} p_{ni}(t_n)\log p_{ni}(t_n) \quad (6)$$

The above described normalization procedure allow us to compare values of the entropy from different outcrops, and of entropy rates from the three selected lava flows.

5. Results

Results of the analysis of the enclaves occurring in the lava flows A, B, and C are shown in Figs. 5 and 6. In the lava flows A and B (Fig. 5a,b), the number of enclaves within each 1×1 m square is nearly constant with the distance from the vent. The variation range is 41–52 m^{-2} (arithmetic mean=48 m^{-2}) in the flow A, and 64–73 m^{-2} (arithmetic mean=69 m^{-2}) in the flow B. The surface area covered by the enclaves in each outcrop is between 872 and 955 cm^2 (arithmetic mean=910 cm^2) in the flow A, and between 965 and 1144 cm^2 (arithmetic mean=1047 cm^2) in the flow B. The average surface area of a single enclave within each 1×1 m square is 18 cm^2 in the flow A, and 15 cm^2 in the flow B. In the lava flow C (Fig. 5c), the number of enclaves varies irregularly between 25 and 78 m^{-2} (arithmetic mean=46 m^{-2}). The surface covered by the enclaves varies also irregularly, and it is between 392

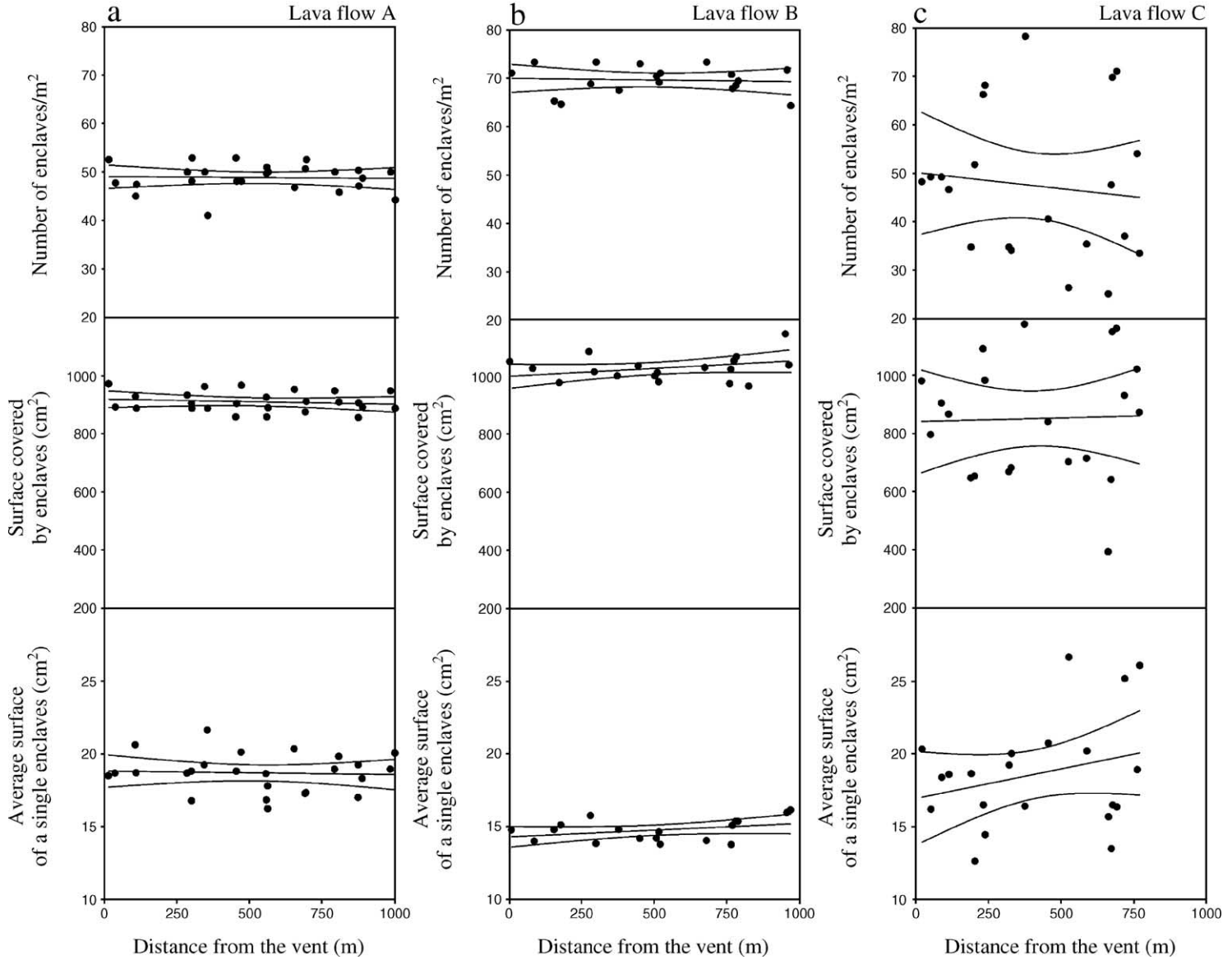

Fig. 5. Variation in the number of the enclaves/m^2, surface covered by the enclaves, and average surface of a single enclave, with the distance from the vent in (a) lava flow A, (b) lava flow B, and (c) lava flow C. Location of the lava flows is in Fig. 1a. The linear interpolations with the 95% confidence are also reported.

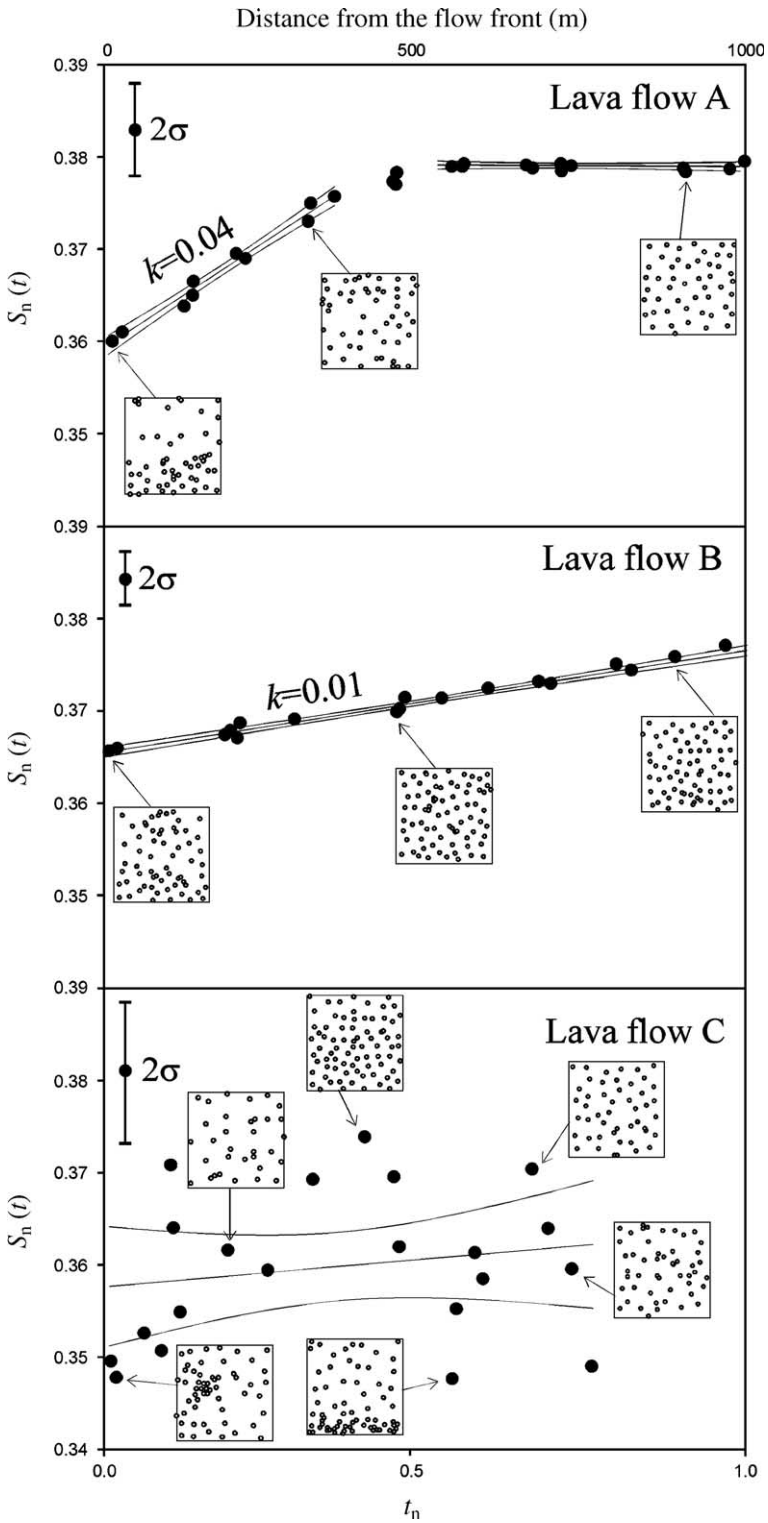

Fig. 6. $S_n(t)$ vs. t_n in (a) lava flow A, (b) lava flow B, and (c) lava flow C. Linear interpolations with the 95% confidence and 2σ are also reported. The distribution of enclaves with linear size ≥ 2 cm (open circles) within selected 1×1 m outcrops (squares) is shown.

and 1176 cm^2 (arithmetic mean = 837 cm^2). The average surface covered by a single enclave is between 12 and 26 cm^2.

The data reported in Fig. 5 show that the values of the geometric parameters of the enclaves from the Porri lavas A and B do not vary appreciably with the distance from the vent (Fig. 5a,b). On the contrary, the parameters of the flow C vary significantly.

Fig. 6 shows the calculated relationships between $S_n(t)$ and t_n. $S_n(t)$ values are between 0.360 and 0.379 in the lava flow A, between 0.366 and 0.378 in lava flow B, and between 0.348 and 0.373 in lava flow C. These values are smaller than those reported in Fig. 3, where $S(t)$ is between −85 and 20. This because the number of points (5000 points) used in the numerical experiments (Fig. 3) is larger than that measured in the field (maximum number 78; Fig. 6). In addition, the entropy values reported in Fig. 6 are calculated using Eq. (2), i.e., a non-normalized form of $S(t)$. On the contrary, the entropy values shown in Fig. 6 are determined using a normalized form of entropy ($S_n(t)$ in Eq. (6)). The reason for the use of a normalized form of entropy to measure the spatial variability of enclaves has been already specified in Section 4. Anyway, the values of $S_n(t)$ calculated for the lava flows A, B, and C are significant within the standard deviation (2σ), as shown in Fig. 6.

In the lava flow A, two main trends may be recognized (Fig. 6). For $t_n < 0.4$, $S_n(t)$ increases following a straight line from 0.36 to 0.377. $S_n(t)/t_n$ is 0.04. For $t_n > 0.5$, $S_n(t)$ maintains a nearly constant value ($S_n(t) \sim 0.379$). In the lava flow B, $S_n(t)$ increases linearly with t_n. $S_n(t)/t_n$ is 0.01. In the lava flow C, unambiguous correlations between $S_n(t)$ and t_n are lacking.

6. Discussion

Results of the analysis of the enclaves of the selected Porri lava flows indicate that, in the flows A and B, there is not variation of the number of enclaves with the distance from the vent (Fig. 5a,b). This implies that significant fragmentation phenomena were lacking during the emplacement of these flows, at least at the scale of observation (10^{-2}–10^{0} m). We conclude that the lava flow kinematics, which is that of a laminar shear flow did not play a major role in the fragmentation of the enclaves, and the observed statistical features in the flows A and B reflect the dynamics of the mingling process between the basaltic andesite and dacite in the reservoir. The virtually constant values of the surface covered by the enclaves, and of the average surface of a single enclave with the distance from the vent suggest that the fraction of the basaltic andesite in the dacite–basaltic andesite mixture did not change during mingling. Therefore, the basaltic andesitic magma was uniformly distributed within the dacitic magma chamber. These observations indicate that the relations between $S_n(t)$ and t_n in the flows A and B (Fig. 6) cannot be ascribed to variations in the fragmentation of the enclaves or to the kinematics of lava flow.

6.1. Lava flow A

The variation of $S_n(t)$ with t_n in the flow A depicts that of chaotic, conservative, mixing dynamical system in a strong regime, according to results from numerical experiments (see Figs. 3 and 6). In particular, the positive linear correlation between $S_n(t)$ and t_n at $t_n < 0.4$, and the near constant value of $S_n(t)$ at $t_n > 0.5$ (Fig. 6) is consistent with the two last stages of the evolution of a fully chaotic mixing system: a second stage in which $S(t)$ is a linear increasing function of time, and a third stage in which $S(t)$ tends asymptotically toward a constant value. As ancillary result, the slope of the straight line in Fig. 6 is the Kolmogorov–Sinai entropy constant $k = dS_n(t)/t_n = 0.04$. k is an indirect measure of the rate of the magma mingling system to reach the homogeneity of the phase space. In summary, we conclude that the lava flow A records two of the three evolution stages of a conservative mingling (mixing) system between a basaltic andesite and a dacite in a strong chaotic regime. From a dynamical point of view, this conclusion implies that (1) the dispersed phase (basaltic andesite) tends progressively to be uniformly distributed within the dacitic host, and, according to the theory on conservative dynamical systems [17,18], the trajectories between early formed, nearby enclaves diverge exponentially with increasing time. These observations suggest that, during the effusion of the lava flow A, efficient stirring and folding processes, i.e., convection, operate within the Porri magma chamber. However, the high viscosity ($\sim 10^6$ Pa s; Table 1) and crystal content (~50 vol.%), of the resident, dacitic magma do not favor convection before the replenishment of the basaltic andesitic magma within the dacite. As a consequence, the convection within the Porri magma chamber must be related to the dynamics of magma mixing. Results from experimental models on magma mixing [35] indicate that injection of a denser and less viscous basaltic magma within a reservoir where a less dense, more viscous and evolved liquid is stored promotes thermal convection. The convective motions drag the

basaltic magma towards the top of the chamber, where the two interacting magma may mingle and, eventually, erupt. This model is able to explain the occurrence of a chaotic dynamics, possibly related to convection, deduced from the analysis of enclaves in the lava flow A. At Porri, we propose that the injection of basaltic andesitic magma in a reservoir where, following Zanon and Nikogosian [31], a resident, crystallizing dacitic magma was stored, induces convection that, in turn, promotes efficient stirring and chaotic advection.

6.2. Lava flow B

In the lava flow B, the recognized linear increase of $S_n(t)$ with t_n does not reflect the multi-stage evolution of a mingling system (Fig. 6). As mentioned before, the constant value of the number of enclaves with the distance from the vent, of the surface covered by the enclaves, and of the average surface of a single enclave indicate that the Liouville's theorem is satisfied. This suggests that if the magma mingling process developed in a chaotic system, then, this system was conservative. Following this hypothesis, the linear increase of $S_n(t)$ with t_n in the flow B could record the second stage of a mingling process in a conservative, fully chaotic, dynamical system, which did not evolve to a third stage. The calculated Kolmogorov–Sinai entropy rate k in the lava flow B is 0.01 (Fig. 6), a value lower than that determined for the second stage of the lava flow A. Therefore, the dispersion of the enclaves of the flow B in the dacitic host occurred with a lower rate with respect to that of the flow A. This hypothesis could explain why the dispersion of the enclaves in the flow B did not reach the homogeneity of the phase space. As alternative hypothesis, the mingling system of the flow B was not fully chaotic. It was at the transition between a strong and weakly chaotic regime, in which the complete homogenization could be never attained [17–19]. This means that the mingling system was at the edge of chaos. The available data (Fig. 6) do not consent to unequivocally favor one of the two above reported interpretations. Anyway, the observed constant increase of $S_n(t)$ in the flow B calls for a chaotic regime.

6.3. Lava flow C

In the lava flow C, the number of enclaves with the distance from the vent, the surface covered by enclaves, and the average surface covered by a single enclave vary irregularly with the distance from the vent (Fig. 5c). Also, there is not correlation between $S_n(t)$ and t_n (Fig. 6). In contrast to the lavas A and B, the above observations indicate that the ratio between the volumes of the basaltic andesite and that of the dacite in the flow C changed with time (see Fig. 5). As a result, the Louville's theorem is not satisfied for the flow C, and if chaotic, it was dissipative mingling system [20,21]. However, the lack of correlations between $S_n(t)$ and t_n suggests that the physical interaction between the two magmas in the flow C occurred in a system in which stirring and folding processes do not operate efficiently. This may be due to: (a) decrease or termination of the convective entrainment within the chamber related to an abrupt decrease or stop of injection of the basaltic andesite within the dacitic magma chamber, and/or (b) abrupt changes in the flow dynamics during the ascent in the conduit related to variation in the effective cross-section of the conduit. In any case, the data from the flow C call for a spatial and temporal inhomogeneity of the mingling system during the eruption.

The results discussed above have some important implications for the dynamics of heterogeneous magmatic systems. Mingled magmas characterized by (a) a homogeneous spatial distribution of enclaves or (b) an initially inhomogeneous distribution evolving towards a homogeneous one testify the occurrence of efficient stirring/stretching and folding processes within the chamber. This process may easily promote chemical homogenization (mixing), depending on the rheological properties of the magmas. On the contrary, mingled magmas with an inhomogeneous distribution of enclaves are indicative of ineffective stirring/stretching and folding. This means that the dynamical interaction between the two magmas, and further mixing, is not allowed.

In the case of the Porri mingling systems studied here, the decrease of k from A to B, and the lack of a measurable k in C, along with the observation that A and B were emitted before C, indicate that the efficiency of advective movements within the Porri magma chamber declined with decreasing time.

The new, analytical approach used here for the analysis of the magma mingling systems of three selected lava flows from the Porri volcano should be extended to other lavas from different volcanoes where there is evidence of interaction between magmas of different composition, and to plutonic environments, where the final stages of mingling processes are preserved. Our results refer to a 2D (surface) analysis of enclaves, and, when possible, a 3D (volume) analysis should be done, possibly using X-ray computed tomography [36]. Finally, the analytical approach used here could be extended.

7. Conclusions

The results of the present study may be summarized in four main points:

(1) The process of physical interaction between magmas of different composition may be analyzed using the approach of statistical mechanics.
(2) The time variation of the statistical entropy, which is a measure of the spatial distribution of the dispersed magma (enclaves), can give information on the efficiency of stirring/stretching and folding processes within the magma chamber, and on the dynamics of the mingling system.
(3) In a chaotic mingling system, the entropy rate may calculated and represents a measure of the rate to reach the spatial uniformity of the phase space. This value could be used to compare the rates of different mingling systems.
(4) A fully chaotic mingling system is characterized by a three stage evolution: an early, initial stage, which is unknown in volcanic environment, a second stage characterized by a linear increase of the statistical entropy with time, and a third stage, in which the uniformity of the system is reached, and the entropy does not vary with increasing time.
(5) Mingled magmas characterized by a uniform spatial distribution of enclaves or by an initially inhomogeneous distribution that evolves towards a homogeneous one testify the occurrence of efficient stirring/stretching and folding processes that may encourage chemical homogenization. Mingled magmas with an inhomogeneous distribution of enclaves indicate that these processes does not play a major role, and the dynamical interaction between the two magmas does not favor further mixing.

Acknowledgments

We would like to thank Ross C. Kerr and anonymous for the useful comments and in-depth reviews that significantly improved the quality of the manuscript. The authors thank Diego Perugini and Giampiero Poli for the numerous discussions on the chaotic behavior of magma mingling systems, and for the co-involvement in the MIUR 2003–2005 project 'Fractal and chaotic reactors: scale invariance and non-linear dynamics in the evolution of magmas'. This study was supported by funding from this MIUR project to GV. We thank also Rosanna De Rosa, Francois Holtz and Roberto Mazzuoli for the discussions on the geology of the Aeolian Islands and on the magma mingling processes at Salina Island.

References

[1] A.R. McBirney, Mixing and unmixing of magmas, J. Volcanol. Geotherm. Res. 7 (1980) 357–371.
[2] C.R Bacon, Magmatic inclusions in silicic and intermediate volcanic rocks, J. Geophys. Res. 91 (1984) 6091–6112.
[3] R.H. Vernon, M.A. Etheridge, V.J. Wall, Shape and microstructure of microgranitoid enclaves: indicators of magma mingling and flow, Lithos 22 (1988) 1–11.
[4] P. Didier, B. Barbarin (Eds.), Enclaves and Granite Petrology, Elsevier, Amsterdam, 1991, 492 pp.
[5] N. Thomas, S.R. Tait, The dimensions of magmatic inclusions as a constraint on the physical mechanism of mixing, J. Volcanol. Geotherm. Res. 75 (1997) 167–178.
[6] M.L. Coombs, J.C. Eichelberger, M.J. Rutherford, Experimental and textural constraints on mafic enclave formation in volcanic rocks, J. Volcanol. Geotherm. Res. 119 (2002) 125–144.
[7] S.R. Paterson, G.S. Pignotta, R.H. Vernon, The significance of microgranitoid enclave shapes and orientations, J. Struct. Geol. 26 (2004) 1465–1481.
[8] G. Iezzi, G. Ventura, The kinematics of lava flows inferred from the structural analysis of enclaves: a review, Special paper 396 'Kinematics and Dynamics of Lava Flows', Geological Society of America, 2005, pp. 15–28.
[9] J.M. Ottino, P. De Roussel, S. Hansen, D.V. Khakhar, Mixing and dispersion of viscous liquids and powdered solids, Adv. Chem. Eng. 25 (2005) 105–204.
[10] J. Muzzio, P.D. Swanson, J.M. Ottino, The statistics of stretching and stirring in chaotic flows, Phys. Fluids A3 (1991) 822–834.
[11] D. Perugini, G. Poli, Chaotic dynamics and fractals in magmatic interaction processes: a different approach to the interpretation of mafic microgranular enclaves, Earth Planet. Sci. Lett. 175 (2000) 93–103.
[12] D. Perugini, G. Ventura, M. Petrelli, G. Poli, Kinematic significance of morphological structures generated by mixing of magmas: a case study from Salina Island (Southern Italy), Earth Planet. Sci. Lett. 222 (2004) 1051–1066.
[13] F. Holtz, S. Lenné, G. Ventura, F. Vetere, Ph. Wolf, Non-linear deformation and break up of enclaves in a rhyolitic magma: a case study from Lipari Island (Southern Italy), Geophys. Res. Lett. 31 (2004), doi:10.1029/2004GL021590.
[14] P. Dutta, R. Chevray, Enhancement of mixing by chaotic advection with diffusion, Exp. Therm. Fluid Sci. 11 (1995) 1–12.
[15] L. Bresler, T. Shinbrot, G. Metcalfe, M.J. Ottino, Isolated mixing regions: origin, robustness and control, Chem. Eng. Sci. 52 (1997) 1623–1636.
[16] P. Gaspard, Chaos, Scattering and Statistical Mechanics. Cambridge Nonlinear Science Series, Cambridge University Press, 1998, 495 pp.
[17] V. Latora, M. Baranger, Kolmogorov–Sinai Entropy Rate versus Physical Entropy, Phys. Rev. Lett. 82 (1999) 520–523.
[18] V. Latora, M. Baranger, A. Rapisarda, C. Tsallis, The rate of entropy increase at the edge of chaos, Phys. Lett. A273 (2000) 97–103.
[19] M. Baranger, V. Latora, A. Rapisarda, Time evolution of thermodynamic entropy for conservative and dissipative chaotic maps, Chaos, Solitons Fractals 13 (2002) 471–478.

[20] S. Sasa, K. Hayashi, Computation of the Kolmogorov–Sinai entropy using statistical mechanics: application of an exchange Monte Carlo method, Europhys. Lett. (in press).
[21] G.F.J. Añaños, F. Baldovin, C. Tsallis, Anomalous sensitivity to initial conditions and entropy production in standard maps: nonextensive approach, Eur. Phys. J. 46 (2005), doi:10.1140/epjb/e2005-00269-1.
[22] B.V. Chirikov, A universal instability of many-dimensional oscillator systems, Phys. Rep. 52 (1979) 264–379.
[23] J. Keller, The Island of Salina, Rend. Soc. Ital. Mineral. Petrol. 36 (1980) 489–524.
[24] D. Barca, G. Ventura, Volcano-tectonic evolution of Salina island (Aeolian Archipelago, South Tyrrhenian Sea), Mem. Soc. Geol. Ital. 47 (1991) 401–415.
[25] R. De Rosa, H. Guillou, R. Mazzuoli, G. Ventura, New unspiked K–Ar ages of volcanic rocks of the central and western sector of the Aeolian Islands: reconstruction of the volcanic stages, J. Volcanol. Geotherm. Res. 120 (2003) 161–178.
[26] R. De Rosa, R. Mazzuoli, G. Ventura, Relationships between deformation and mixing processes in lava flows: a case study from Salina (Aeolian Islands, Tyrrhenian Sea), Bull. Volcanol. 58 (1996) 286–297.
[27] G. Ventura, R. De Rosa, R. Mazzuoli, E. Colletta, Deformation patterns in high-viscous lava flows inferred from the preferred orientation and tiling of crystals. An example from Salina (Aeolian Islands, Southern Tyrrhenian Sea-Italy), Bull. Volcanol. 57 (1996) 555–562.
[28] G. Ventura, Kinematic significance of mingling–rolling structures in lava flows: a case study from Porri Volcano (Salina, Southern Tyrrhenian Sea), Bull. Volcanol. 59 (1998) 394–403.
[29] G. Ventura, The strain path and emplacement mechanism of lava flows: an example from Salina (Southern Tyrrhenian Sea, Italy), Earth Planet. Sci. Lett. 188 (2001) 229–240.
[30] E. Colletta. Studio petrografico e geochimico della sequenza eruttiva del I Ciclo di attivita' del Mte dei Porri (Isola di Salina—Arcipelago delle Eolie), Thesis (1993), University of Calabria Italy.
[31] V. Zanon, I. Nikogosian, Evidence of crustal melting events below the Island of Salina; Aeolian Arc, Southern Italy, Geol. Mag. 141 (2004) 525–540.
[32] S. Blake, J.H. Fink, On the deformation and freezing of enclaves during magma mixing, J. Volcanol. Geotherm. Res. 95 (2000) 1–8.
[33] Q. Williams, O.T. Tobish, Microgranitic enclave shapes and magmatic strain histories: constraints from drop deformation theory, J. Geophys. Res. 99 (1994) 24359–24368.
[34] L. Mastin, M.S. Ghiorso, A Numerical Program for Steady-State Flow of Magma–Gas Mixtures Through Vertical Eruptive Conduits, U.S.G.S. Open-File Report, 2000, pp. 1–209.
[35] D. Snyder, S. Tait, Magma mixing by convective entrainment, Nature 379 (1996) 529–531.
[36] W.D. Carlson, C. Denison, R.A. Ketcham, High-resolution X-ray computed tomography as a tool for visualization and quantitative analysis of igneous textures in three dimensions, Electron. Geosci. 3 (1999) 1–14.